

Molecular Dynamics Simulation of Crack Propagation in Polycrystalline Material

K. Nishimura¹ and N. Miyazaki²

Abstract: In this paper, we present a classical molecular dynamics algorithm and its implementation on Cray C90 and Fujitsu VPP700. The characters of this algorithm consist in a grid based on the block division of the atomic system and a neighbor list based on the use of a short range potential. The computer program is used for large scale simulations on a Cray C90 and a 32-node VPP700, and measurements of computational performance are reported. Then, we examine the interaction between a crack propagating and a tilt grain boundary under uniaxial tension using this computer program. The Johnson potential for α -Fe is used in these simulations. A structural transition from bcc to hcp induced by hydrostatic stress and brittle crack propagation are observed in a system including a crack whose direction is [010] in the (101) plane. In a system including both the crack and a [110](112) grain boundary which is symmetric and stable, not only the phase transition but also crack propagation is restrained by the grain boundary. In a system including both the crack and a [110](111) grain boundary which is asymmetric and unstable, intergranular crack propagation occurs after the crack tip reaches the grain boundary.

keyword: Molecular Dynamics, Brittle Fracture, Crack Propagation, Grain Boundary, α -Fe.

1 Introduction

The evaluation of material properties has been recently executed from the viewpoint of micro scale for the purpose of the application to the analysis of semiconductor manufacture process and structural design of a micromachine. A molecular dynamics method can estimate the mechanical properties of materials by an atomic level. It could be the alternative approach different from conventional continuum mechanics.

Recently we can deal with a large molecular dynamics

system over 10 millions atoms as a result of the rapid development of computer technology and the establishment of parallel processing. Zhou, Lomdahl, Voter and Holian (1998) dealt with a system of 35 millions atoms to discuss the emission of dislocations from a three-dimensional crack in copper. Abraham and Broughton (1998) made a molecular dynamics analysis of a system of 10 millions atoms and discovered that crystal orientation with respect to the uniaxial loading is important. These studies, however, dealt with only single crystal materials. Considering that almost all practical materials are polycrystalline, we should examine the effect of grain boundaries on the strength of materials. Saitoh, Kitagawa, Nakatani and Ogata (1997) examined the strength of a grain boundary in aluminum using coincidence site lattice model, and discussed the fracture energy of a grain boundary and the effect of boundary conditions on the failure behavior. Moreover a molecular dynamics method has been applied to a system including both a crack and a grain boundary. Zhang and Wang (1996) examined the interaction between a dislocation array emitted from a crack tip and a grain boundary for a copper subjected to mode II loading, and clarified the initial phase of ductile fracture in a polycrystalline material. The fracture of face centered cubic (fcc) metals occurs in a ductile manner, but brittle fracture occurs in almost all body centered cubic (bcc) metals and alloys. However, there has been no study on the interaction between a crack propagating in a brittle manner and a grain boundary.

In this paper, we discuss the effect of a grain boundary on brittle crack propagation process for α -Fe, a bcc metal, and clarifies the initial stage of brittle fracture in a polycrystalline material. We perform a molecular dynamics analysis of a system including only a crack subjected to mode I loading to observe brittle crack propagation process. We also perform the analysis of a system including both a crack and a grain boundary to examine the effect of a grain boundary on crack propagation. In this analysis, we consider two kinds of grain boundaries, that is, a

¹ Kyushu National Industrial Research Institute, Saga, JAPAN.

² Kyushu University, Fukuoka, JAPAN.

symmetric and stable one and an asymmetric and unstable one.

2 Method of Analysis

2.1 Molecular dynamics method

In the molecular dynamics method, a material is modeled as a multi-particle system which is governed by the classical mechanics. The particles or atoms move by receiving forces from other particles, and the particle or atom motion is expressed by the Newton's law of motion as follows :

$$m_i \frac{d^2 \mathbf{x}_i}{dt^2} = \mathbf{F}_i \left(= \sum_{j=1, j \neq i}^N \frac{\partial \phi_{ij}}{\partial \mathbf{r}_{ij}} \frac{\mathbf{r}_{ij}}{r_{ij}} \right) \quad (1)$$

where m_i is the mass of the i -th atom, \mathbf{x}_i is the position vector of the i -th atom, \mathbf{F}_i is the force vector acting on the i -th atom, ϕ_{ij} is the inter atomic potential, \mathbf{r}_{ij} is the vector from the i -th atom to the j -th atom and r_{ij} is its length. Eq. 1 can be solved as an initial-value problem of ordinary differential equations, if initial conditions for position and velocity are prescribed to all atoms. We employ a numerical technique to solve the Eq. 1, because a multi-body problem cannot be solved analytically. We execute explicit numerical integral using an appropriate time step and solve position and velocity of each atom at an arbitrary time. We use the velocity Verlet method as a time integral method. Initially we allocate the atoms at the bcc lattice positions and give the velocities of the atoms which follows the Maxwell distribution at a prescribed temperature.

We use the Johnson potential for α -Fe, see Johnson (1964). The Johnson potential is a short range pair potential which has a cut-off distance, within which the second-nearest neighbor atoms are included. After providing strain to a system, we use a canonical ensemble which keeps the volume and temperature of the system constant. We assume that the system is conceptually connected to a heat bath which operates to keep the system temperature constant by exchanging energy with a system. We use the velocity scaling method to keep the system temperature constant. In this method, the velocities of the atoms are scaled to a prescribed temperature at each time step. We use the neighboring list method to reduce computational time. In this method, each atoms has

a list of partner atoms which are located within the cut-off distance, and a member of calculation for the force acting on the atoms can be greatly reduced. Table 1 shows algorithm for the molecular dynamics simulation.

Table 1 : Algorithm for molecular dynamics simulation

time integral	velocity Verlet method
initial position	body centered cubic
initial velocity	Maxwell distribution
potential	Johnson potential
temperature control	velocity scaling method

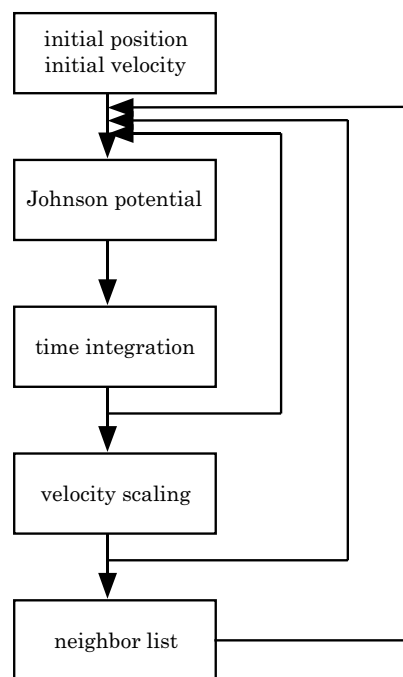


Figure 1 : Flow chart for molecular dynamics simulation

2.2 Neighbor list method of block division type

In case of dealing with a large scale system, it is important to estimate how much the computational time of each part of a program increases with the increase of the number of atoms in the system. When we consider each part of the molecular dynamics program shown in Fig. 1, the computational times except for the neighbor list are $O(N)$, where N indicates the number of atoms. On the other hand, the computational time for the neighbor list

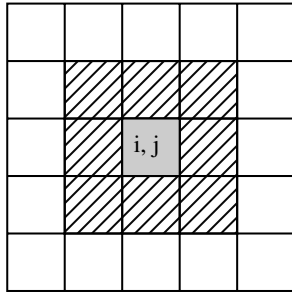


Figure 2 : Neighbor list method of block division type

is $O(N^2)$, because we calculate respective inter-atomic distances for all atoms in the system. Thus, in case of a large scale system, the total computational time would be dominated by the computational time for the neighbor list. So we propose an algorithm which reduces the computational time for the neighbor list to $O(N)$. We call it the neighbor list method of block division type.

In the proposed algorithm, we restrict the number of atoms to calculate inter-atomic distances. We explain this algorithm for a two-dimensional system. We divide the system into some blocks, as shown in Fig. 2. Then using the initial position of atoms, we set the number of each atom belonging to the block (i,j) into an array. When we draw up the neighbor list, we calculate the distance only between each atom in the block indicated in gray in Fig. 2 and that in the 8 contiguous blocks indicated as hatched regions in Fig. 2. Then we judge whether the calculated inter-atomic distance is registered in the neighbor list or not. In a three-dimensional case, the number of contiguous block is 26. We assume in this algorithm that the position of each atom does not change too much from its initial position. This assumption can be applied to atoms in a solid.

2.3 Mask method

Real materials have complex internal structures such as voids, cracks and precipitation particles. It is not easy to model such complex internal structures in MD simulations. We propose a method describing complex internal structures in a simple manner. We call it the mask method. As described in 2.2, a physical space is divided into some blocks in order to apply the neighbor list method of block division type. We provide a mask array for each block, which describes the status of the

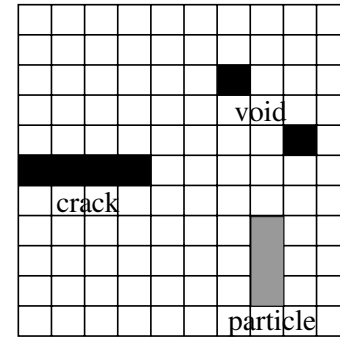


Figure 3 : Mask method

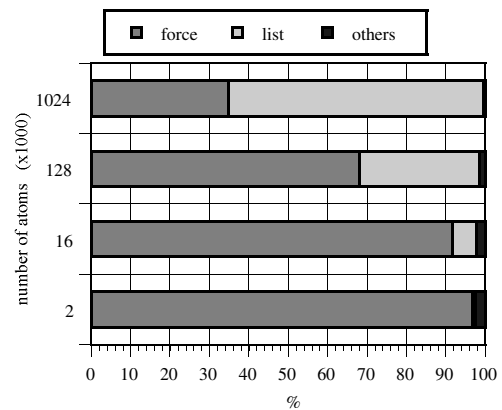


Figure 4 : Time consumption rate in subroutines on Cray C90 using conventional algorithm

block. For example, we do not take account of the interaction of atoms for the black parts in Fig. 3 which can model a crack or a void. On the other hand, we employ another potential for the gray part in Fig. 3, which is different from that of the white part, in order to represent a precipitation particle.

3 Evaluation of Computational Performance

3.1 Analyzed system

We evaluate the performance of the proposed algorithm. α -Fe is analyzed at the temperature of 300K. The size of one block is $2a \times 2a \times 2a$ where a denotes the lattice constant, and 432 atoms are searched for drawing up a neighbor list. We perform a MD simulation for 10000 time steps, controlling the system temperature every 500 time steps and renewing the neighbor list every 5000 time steps.

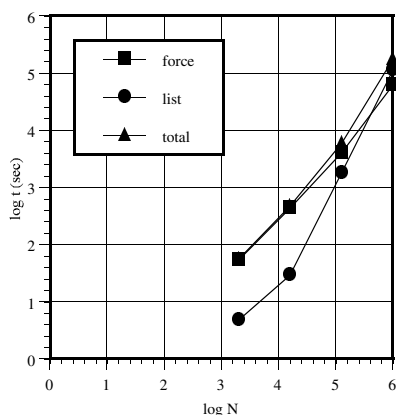


Figure 5 : Computational time on Cray C90 using conventional algorithm

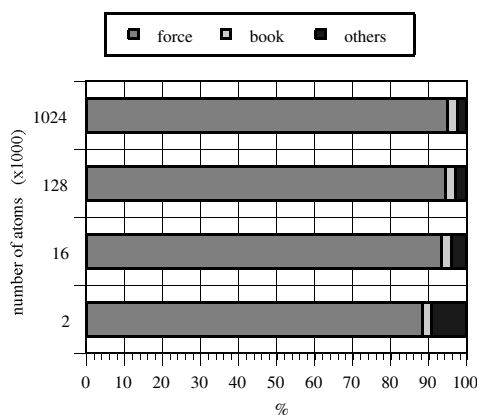


Figure 6 : Time consumption rate in subroutines on Cray C90 using block division algorithm

3.2 Computer systems using in the calculation

In this study, we use two kinds of computer systems which have different hardware architectures respectively and evaluate the performance of our molecular dynamics program. One is a computer system of vector type with a sheared memory and another is that of vector parallel type with distributed memories. The former is Cray C90 with tightly coupled 16 processors and an SRAM sheared memory. The theoretical maximum processing performance is 16 GFLOPS or 1 GFLOPS per processor. The size of a main memory is 8 GB and 4 GB memory is available for one job. The latter is Fujitsu VPP700 Model 56 with loosely coupled 56 processors which have own memory. The theoretical maximum processing performance is 123 GFLOPS or 2.2 GFLOPS per processor. The size of a main memory is 112 GB and 54 GB memory is available for one job.

3.3 Evaluation of the performance on Cray C90

At first, we will show the results obtained by the computer program based on the conventional algorithm using Cray C90. Fig. 4 shows the time consumption rate in each subroutine which is defined by the rate of computational time in each subroutine to the total computational time. The numbers of atoms are 2000, 16000, 128000 and 1024000. In Fig. 4, “force” represents the subroutine for calculating the force acting on each atom from other atoms using the Johnson potential, “list” represents the subroutine for drawing up the neighbor list based on the Verlet neighbor list method, and “others” represents

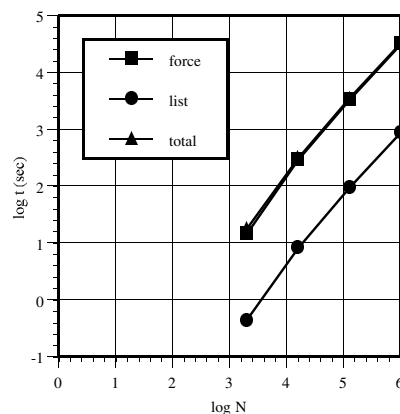


Figure 7 : Computational time on Cray C90 using block division algorithm

the subroutines for performing time integral based on the velocity Verlet method, temperature control based on velocity scaling method and so on. We can find from this figure that the rate of the computational time for drawing up the neighbor list to the total computational time increases with the increase of the number of atoms. Fig. 5 shows the relations between the total computational time t and the number of atoms N . The computational time for drawing up the neighbor list is almost negligible, compared with the total computational time, when the number of atoms is small. As the number of atoms increases, it increases and becomes dominant when N is 1024000. We find the linear relationship between $\log t$ and $\log N$ with the slope of about one for “force” and with that of about two for “list”. Accordingly, the computational time

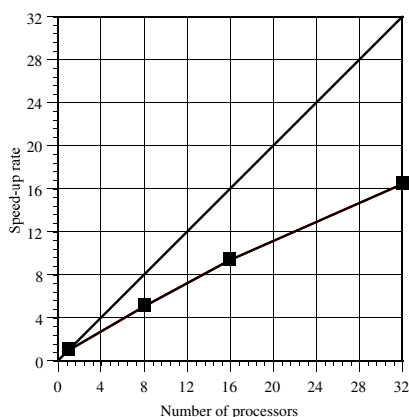


Figure 8 : Speed-up rate on VPP77

for calculating force acting on atoms increases by $O(N)$, while that for drawing up the neighbor list increases by $O(N^2)$ and the total computational time increases rapidly with the increase of N .

We employ the neighbor list method of block division type to reduce the computational time for drawing up the neighbor list. The results obtained by the improved algorithm are respectively shown in Fig. 6 and Fig. 7 for the time consumption rate in each subroutine and for the relations between total computational time t and the number of atoms N . The time consumption rate in each subroutine keeps nearly constant irrespective of increasing the number of atoms. Both the computational times for calculating the force acting on atoms and that for drawing up the neighbor list increase by $O(N)$ and the rapid increase in the total computational time cannot be found. When the number of atoms is 1024000, the total computational times are respectively 1.77×10^5 seconds for the conventional algorithm and 3.23×10^4 seconds for the improved algorithm. Therefore, newly proposed method is five times faster than the conventional method.

3.4 Evaluation of the performance on Fujitsu VPP700

We execute our molecular dynamics program using the neighbor list method of block division type on Fujitsu VPP700. Because the computational time for calculating the force acting on atoms is dominated as shown in Fig. 6, we parallelize the loop for the force calculation by data parallel method. The speed-up rate for parallel processing is shown in Fig. 8 in case of $N=1024000$, the abscissa

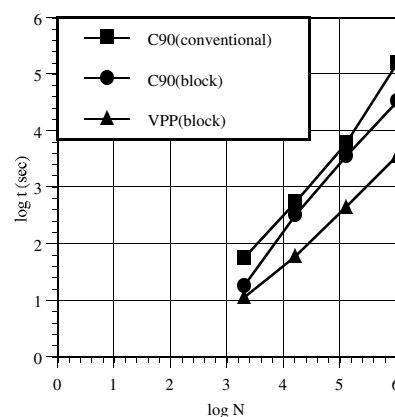


Figure 9 : Computational time in respective cases

and ordinate of which indicate the number of processors and the speed-up rate which means the increase in processing speed of multi-processor compared with that of one processor, respectively. In this figure, the solid diagonal line shows the theoretical speed-up rate. We can find from this figure that the actual speed-up rate is less than the theoretical one. If the efficiency is defined by the rate of actual speed-up rate to the theoretical one, it reduces with the increase in the number of processors. That is, the efficiency is 63% for 8 processors, 57% for 16 processors and 51% for 32 processors. The reduction of the efficiency is due to the increase in the rate of data communication among processors. When we use 32 processors, the speed-up rate is 16 and the total computational time is 3.5×10^3 seconds. So we can execute a molecular dynamics calculation practically with reasonable computational time.

The relations between total computational time and the number of atoms are shown in Fig. 9 for three cases, that is, the conventional neighbor list method on Cray C90, the neighbor list method of block division type on Cray C90 and the neighbor list method of block division type on Fujitsu VPP700 with 32 processors. We can see that the total computational time increases by $O(N)$ for the last case. In summary, VPP700 is about ten times faster than C90 and the neighbor list method of block division type proposed by us is about five times faster than the conventional neighbor list method.

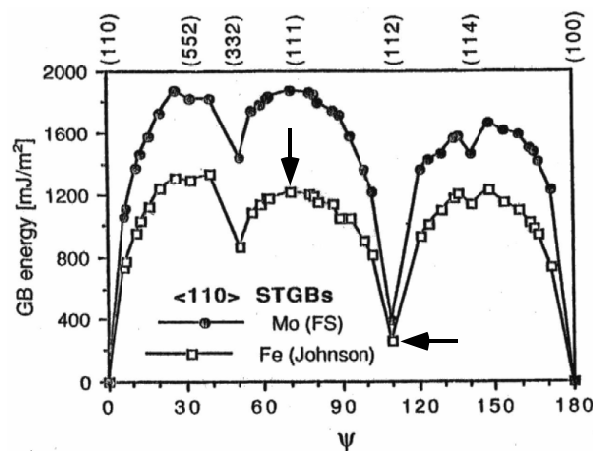


Figure 10 : Energy of [110] symmetrical tilt grain boundaries in Mo(FS) and Fe(Johnson) obtained by Wolf and Merkle (1992)

4 Crack Propagation Analysis

We perform molecular dynamics analyses of crack propagation using the aforementioned computer program. The computer used is the VPP700.

4.1 Grain boundary model

A polycrystal has grain boundary structures, which are characterized by the relative orientation of two single crystal regions adjacent to a grain boundary. There have been a lot of studies using a molecular dynamics simulation on the evaluation of grain boundary energy and on the grain boundary structure. Wolf and Merkle (1992) calculated the grain boundary energy of a tilt grain boundary in Mo and Fe, bcc metals, by changing misorientation angle. They used the EAM potential for Mo and the Johnson potential for Fe. The result is shown in Fig. 10 where the abscissa is misorientation angle, and the ordinate is grain boundary energy. The direction of the axis of misorientation angle is [110]. The grain boundaries corresponding to the local minimum in Fig. 10 are symmetric and stable. They are the coincidence grain boundaries. In this study, we choose two kinds of grain boundaries. One is a grain boundary whose misorientation angle is about 110 degrees and the grain boundary surface is the (112) plane. It is a symmetric and stable grain boundary and we call it the [110](112) grain boundary. The other is a grain boundary whose misorientation angle is about 70 degrees and grain

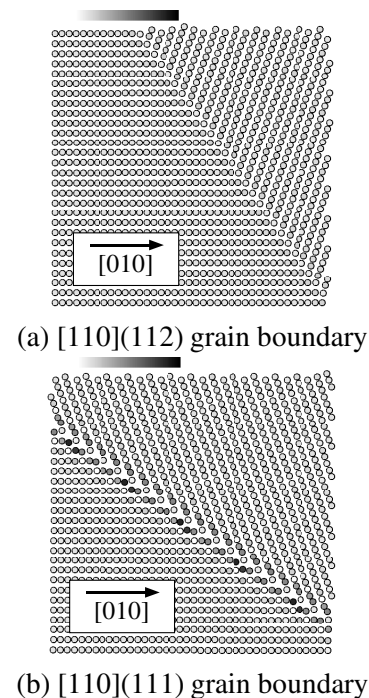


Figure 11 : Snapshots for a [110](112) grain boundary and a [110](111) grain boundary

boundary surface is the (111) plane. It is an asymmetric and unstable grain boundary and we call it the [110](111) grain boundary. These two kinds of grain boundaries are in Fig. 10 by arrows.

Fig. 11 shows snapshots around the grain boundaries for the [110](112) grain boundary and the [110](111) grain boundary after relaxation. The gray-scale of the atoms in Fig. 11 indicates the potential energy level of each atom, which is normalized by the absolute value at the minimum point of the Johnson potential. The [110](112) grain boundary shows good lattice consistency around the grain boundary and almost the same potential energy level as a bulk region. On the other hand, the [110](111) grain boundary shows poor lattice consistency around the grain boundary and higher potential energy level at several layers around the grain boundary than a bulk region.

4.2 Analysis model and calculation conditions

Fig. 12 shows the relationship between the lattice directions and a coordinate system of a crack. We deal with the in-plane opening or mode I deformation of a crack whose surface and direction correspond to the (101) plane the [010] direction, respectively. The [111]

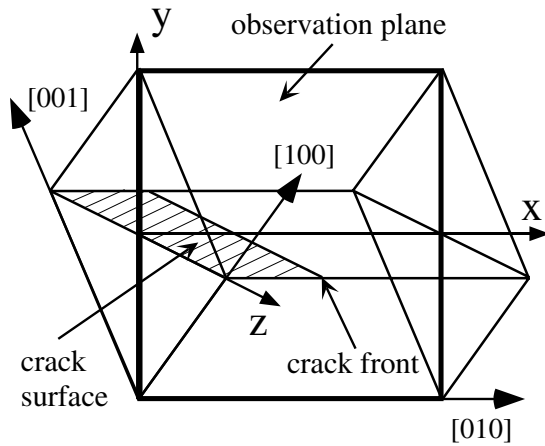


Figure 12 : Lattice direction and crack surface

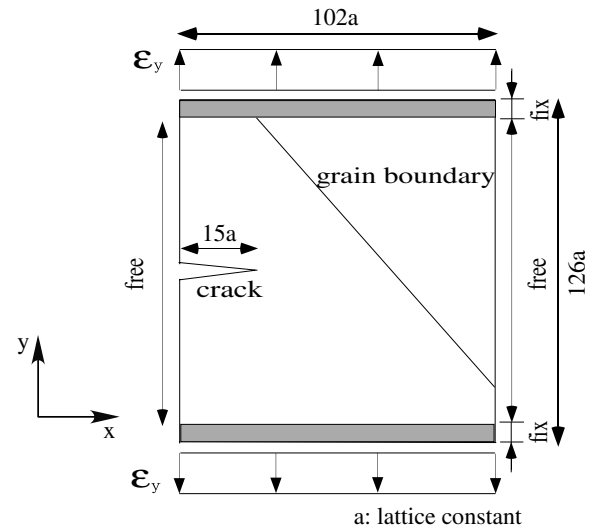


Figure 13 : Boundary conditions

direction, a primary slip direction of the bcc structure, is included in this plane. The (110) plane is known as a cleavage surface of α -Fe. We can expect that cleavage fracture would occur easily because a cleavage surface coincides with a crack surface. The (101) plane indicated by bold lines in Fig. 12 is an observation plane, at which the results of the molecular dynamics simulations are shown. The x-y-z coordinate system shown in Fig. 12 is taken in such a way that the x-axis coincides with the crack direction, and the y-axis is normal to the crack surface, and the z-axis is normal to the observation plane.

The boundary conditions are shown in Fig. 13. Vertical boundaries are free surfaces, and four atomic layers along the upper and lower horizontal boundaries are fixed to apply mode I loading to the system. A periodic boundary condition is imposed on the six layers along the z-axis. A crack length is $15a$ where a denotes the lattice constant. Four atomic layers are removed to introduce a crack in order that a radius of curvature at a crack tip may become nearly the lattice constant. A grain boundary is introduced, as shown in Fig. 13. It divides the analysis domain into two parts. The atoms are moved not only in the y-direction but also in the x-direction in order to give mode I loading. At the first step, we obtain a stable structure at the strain ϵ_y of 0.03 after performing the calculation of 100000 steps for relaxation. Crack propagation does not occur at this strain level. Then ϵ_y is increased from 0.03 to 0.07 and a molecular dynamics simulation is performed at ϵ_y of 0.07. At this strain level,

crack propagation occurs and we observe the crack propagation behavior and interaction between a propagating crack and a grain boundary. All the molecular dynamics simulations are performed at the temperature of 300 K.

5 Simulation Results and Discussion

5.1 A system including only a crack

In this section, we show the results of the analysis for a system including only a crack subjected to mode I loading. Fig. 14 shows a snapshot around a crack tip immediately after crack propagation starts. In the figure, the atoms in the two layers of the z-direction are shown together with a gray scale representing a hydrostatic pressure level of each atom. Stress concentration occurs near the crack tip and the stress σ_y at the crack tip is equal to 34.52 GPa. This value agrees well with the ideal cleavage strength of the (110) plane for α -Fe, 34.88 GPa, which was evaluated by Yanagida and Watanabe (1996) using the Johnson potential. Around the crack tip, there is a domain where the crystal structure differs from bcc. In this domain, we can observe stress relaxation and hexagonal atomic structures like stacking triangle lattices. We also confirm that the stacking structure of the z-direction is ABABAB. Stress concentration can be observed in the front periphery of this domain, at which hydrostatic pressure is about 13 GPa.

Change of crystal structure for Fe under high pressure

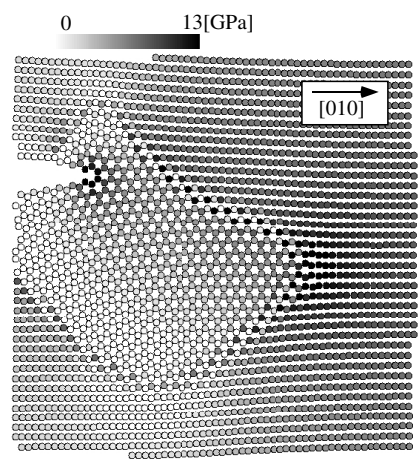


Figure 14 : A snapshot for a crack tip in a system including only a crack

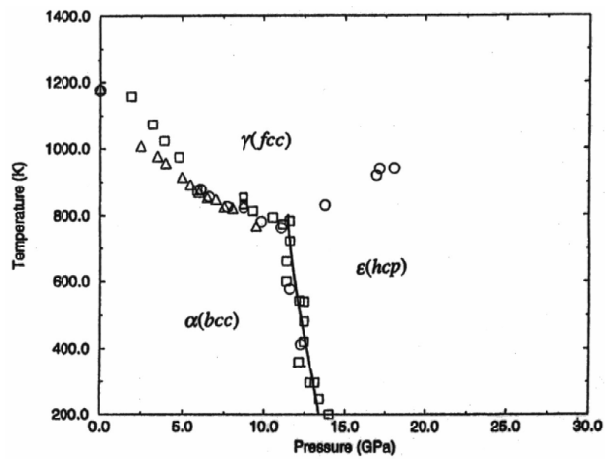


Figure 15 : Iron phase diagram obtained by Boettger and Wallace (1996)

has been clarified experimentally. Fig. 15 shows the phase diagram for Fe given by Boettger and Wallace (1996). We can find from this figure that phase transition from α -Fe, the bcc structure, to ϵ -Fe, the hexagonal close-packed (hcp) structure, occurs at hydrostatic pressure of about 13 GPa when pressure increases, keeping temperature at 300 K. Cheung, Harrison and Yip (1992) also proposed a phase transition mechanism for Fe under uniaxial tensile stress using a molecular dynamics simulation. According to their study, phase transition from bcc to hcp results from homogeneous shear and atomic shuffling, and the reverse transition results from only homogeneous shear without atomic shuffling. Wang and

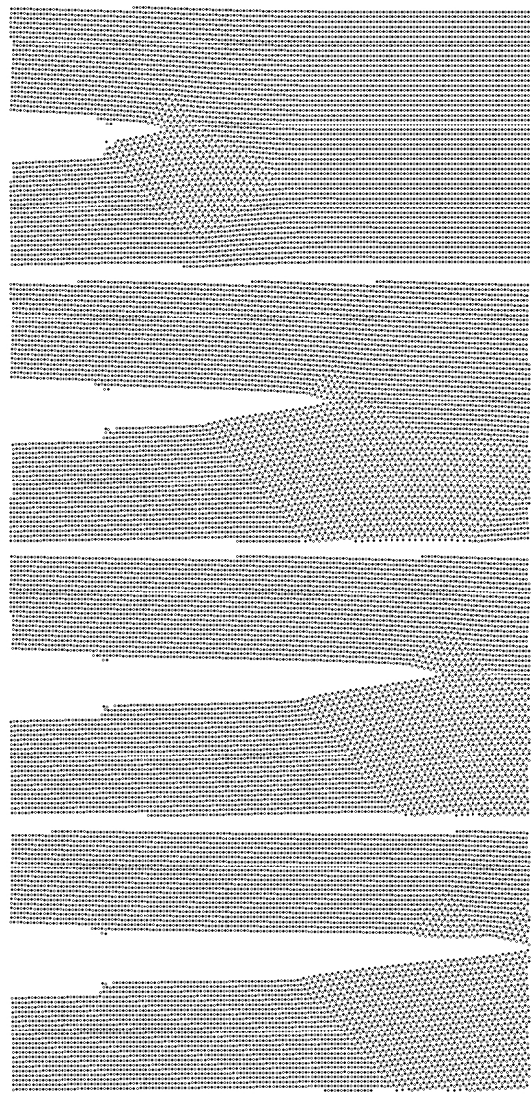


Figure 16 : Snapshots for crack propagation process in a system including only a crack

Ingalls (1997) performed an experimental study to measure the lattice constant of ϵ -Fe, and clarified hysteresis of the phase transition. Considering the previous studies mentioned above, we can conclude that the domain around the crack tip whose crystal structure differs from bcc is ϵ -Fe, the hcp structure, induced by high hydrostatic pressure which results from stress concentration around the crack tip. Hereafter we call it the phase transition domain.

Several snapshots for crack propagation process are shown in Fig. 16. The atoms in the two layers of z-direction are shown in the figure, where the black atoms

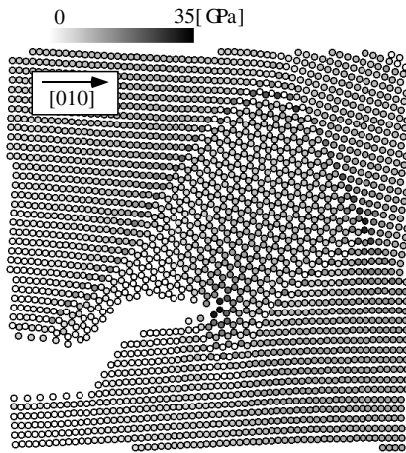


Figure 17 : A snapshot for interaction between crack propagation and a [110](112) grain boundary

and white ones indicate that they exist in different layers, respectively. The phase transition from α -Fe to ϵ -Fe occurs at the crack tip due to stress concentration around the crack tip and the crack propagates together with the phase transition domain around the crack tip, expanding the phase transition domain toward the direction of crack propagation. Reverse phase transition from ϵ -Fe to α -Fe as pointed out by Wang and Ingalls (1997) can be observed due to the stress relaxation after the crack tip passes by. We confirm that the stress σ_y at the crack tip during crack propagation process is in good agreement with the ideal cleavage strength. Conclusively, cleavage fracture occurs and the crack propagates brittly without plastic deformation.

5.2 A system including both a crack and a [110](112) grain boundary

Here we show the results of the analysis for a system including both a crack and a [110](112) grain boundary subjected to mode I loading. Fig. 17 shows a snapshot around a crack tip when the crack tip comes to near the grain boundary shown in the upper right-hand corner in the figure. The atoms in the two layers of the z-direction are shown in this figure together with a gray scale representing the stress σ_y of each atom. The value of the stress σ_y at the crack tip is 33.70 GPa which agrees well with the ideal cleavage strength. The phase transition domain spreads from the crack tip to the grain boundary, but it cannot spread beyond the grain boundary. Although the

direction of crack propagation is [010] in the (101) plane in case of the system including only a crack, as shown in 5.1, it changes from [010] to the slip direction [111] during crack propagation process in the present case. That is, cleavage fracture occurs not only in the (101) plane but also in the slip plane (121).

Fig. 18 shows snapshots for crack propagation process. The atoms in the two layers of z-direction are shown in the figure, where the black atoms and white ones indicate that they exist in different layers, respectively. The crack propagates together with the phase transition domain around the crack tip. The size of the phase transition domain is smaller in the present case than in the former case, that is, the system including only a crack. After the phase transition domain reaches the grain boundary, it cannot expand beyond the grain boundary. So it could be concluded that the [110](112) grain boundary prevents the phase transition. The width of the grain boundary increases during crack propagation process, but fracture does not occur in the band of the grain boundary. After the crack tip reaches the grain boundary, the crack propagates initially in the band of the grain boundary, but it is arrested finally. It can be therefore concluded that the [110](112) grain boundary has the effect of preventing brittle crack propagation because it has low grain boundary energy and is symmetric and stable.

5.3 A system including both a crack and a [110](111) grain boundary

In this section, we show the results of the analysis for a system including both a crack and a [110](111) grain boundary subjected to mode I loading. Fig. 19 shows snapshots for crack propagation process. The atoms in the two layers of z-direction are shown in the figure, where the black atoms and white ones indicate that they exist in different layers, respectively. In the beginning of crack propagation, the phase transition domain is induced near the crack tip. As in case of the [110](112) grain boundary, we can find that the grain boundary suppresses the expansion of the phase transition domain. The crack propagates along the [010] direction in the (101) plane. Meanwhile, a new crack is generated at the grain boundary, growing to a long intergranular crack, and these two cracks coalesce into a long new crack. Then this crack propagates along the grain boundary. Crack propagation process is brittle fracture. Conclusively, the [110](111) grain boundary has high grain boundary energy and is

asymmetric and unstable so that it cannot prevent brittle crack propagation.

6 Conclusions

We performed molecular dynamics simulations of α -Fe to examine the effect of a grain boundary on crack propagation. In the present simulations, we dealt with a crack whose direction is [010] in the (101) plane subjected to mode I loading and two kinds of grain boundaries, that is, the [110](112) grain boundary and the [110](111) grain boundary. We also performed a molecular dynamics simulation of a system without a grain boundary for comparison. The following are conclusions derived from the present study.

- (1) The phase transition from α -Fe, bcc, to ϵ -Fe, hcp, is observed around a crack tip. This phase transition is induced by high hydrostatic pressure which results from stress concentration around the crack tip.
- (2) The stress σ_y at the crack tip during crack propagation process is in good agreement with the ideal cleavage strength of α -Fe. So cleavage fracture occurs when the stress σ_y at the crack tip exceeds this ideal strength and the crack propagates brittlely without plastic deformation.
- (3) The [110](112) grain boundary has the effect of preventing brittle crack propagation because it has low grain boundary energy and is symmetric and stable.
- (4) The [110](111) grain boundary has high grain boundary energy and is asymmetric and unstable so that it cannot prevent brittle crack propagation.

References

- Zhou, S. J., Lomdahl, P. S., Voter A. F. and Holian B. L.** (1998): Three-dimensional fracture via large-scale molecular dynamics. *Eng. Fract. Mech.*, 61, 173-187.
- Abraham, F.F. and Broughton J.Q.** (1998): Large-scale simulations of brittle and ductile failure in fcc crystals. *Comp. Mater. Sci.*, 10, 1-9
- Saitoh, K., Kitagawa, H., Nakatani, A. and Ogata, S.** (1997): Molecular dynamics study on strength of coincidence grain boundaries. *J. Soc. Mater. Sci., Jpn.*, 46, 238-243.
- Zhang, Y. W. and Wang, T. C.** (1996): Molecular dynamics simulation of interaction of a dislocation array from a crack tip with grain boundaries. *Modeling Simul. Mater. Sci. Eng.*, 4, 231-244.
- Johnson, R. A.** (1964): Interstitials and Vacancies in α -Iron. *Phy. Rev.* 134, 1329-1336.
- Wolf, D. and Merkle, K. L.** (1992): Materials Interface. *Correlation between the structure and energy of grain boundaries in metals*, Chapman & Hall, 87-150
- Yanagida, N. and Watanabe, O.** (1996): Molecular Dynamics Simulation of Effects of Lattice Orientation on Crack Propagation in Alpha-Iron when the Primary Slip Direction is in the Plane of Tensile Stress. *JSME Int. J.*, ser. A, 39, 321-329.
- Boettger, J. C. and Wallace, D. C.** (1996): Metastability and dynamics of the shock-induced phase transition in iron. *Phy. Rev. B*, 55, 2840-2849.
- Cheung, K. S., Harrison, R. J. and Yip, S.** (1992): Stress induced martensitic transition in a molecular dynamics model of α -iron. *J. Appl. Phys.*, 71, 4009-4014
- Wang, F. M. and Ingalls, R.** (1997): Iron bcc-hcp transition: Local structure from x-ray-absorption fine structure. *Phy. Rev. B* 57, 5647-5654.

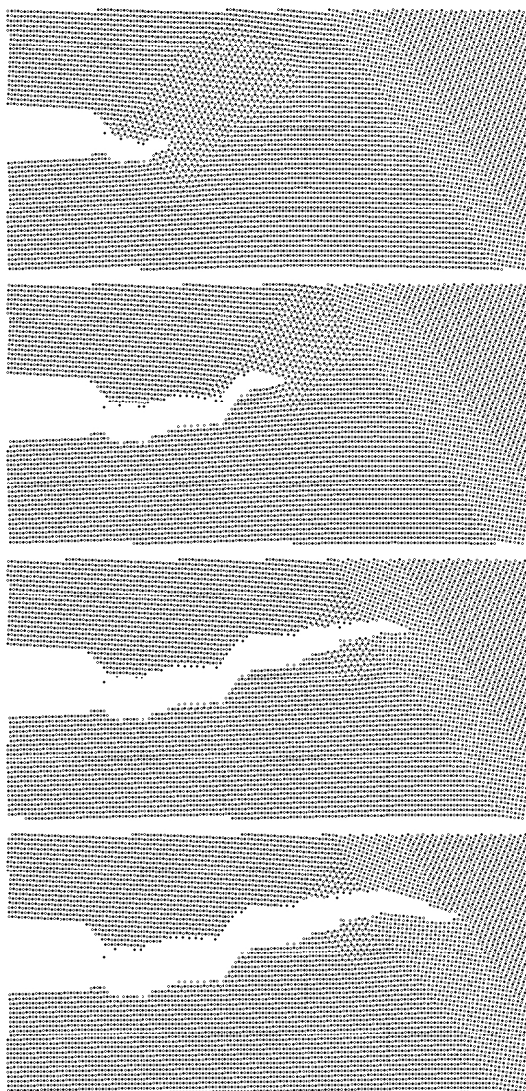


Figure 18 : Snapshots for crack propagation process in a system including both a crack and a [110](112) grain boundary

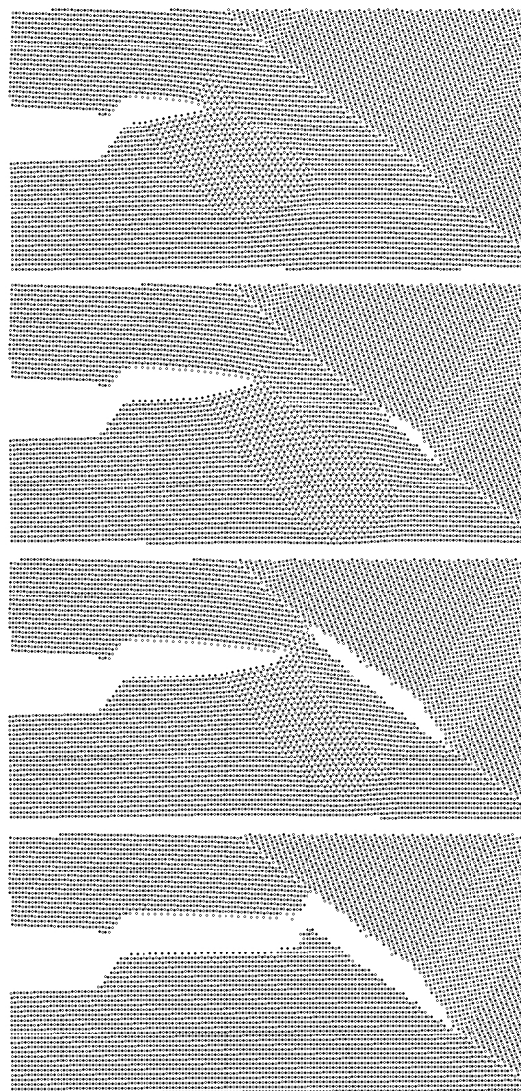


Figure 19 : Snapshots for crack propagation process in a system including both a crack and [110](111) grain boundary

